Scripta Materialia 250 (2024) 116192

Contents lists available at ScienceDirect

Scripta Materialia

journal homepage: www.journals.elsevier.com/scripta-materialia

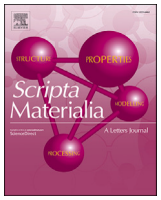

Bicontinuous microstructure formation through partial melting

Zhongyang Li [a], Lukas Lührs [a], Jörg Weissmüller [a,b,*]

[a] Institute of Materials Physics and Technology, Hamburg University of Technology, Hamburg, Germany
[b] Institute of Hydrogen Technology, Helmholtz-Zentrum Hereon, Geesthacht, Germany

ARTICLE INFO

Keywords:
Dealloying
Grain boundary wetting
Cu-In alloy
Bicontinuous structure
Interpenetrating-phase microstructures
Liquid-metal dealloying
Discontinuous reaction by interface migration

ABSTRACT

Liquid-metal dealloying generates porous metals or interpenetrating-phase composites. Particularly attractive is the use of the alloy's innate melt for activating dealloying throughout the bulk, even in extended sample geometries, during reverse peritectic melting. We explore if interpenetrating-phase microstructures may be observed more generally during partial melting of solid solutions with an extended temperature interval of solid-melt coexistence. Incomplete wetting of grain boundaries by the melt is then a prerequisite for a bicontinuous structure. For a Cu-In alloy, we show that special grain boundaries remain non-wetted and provide a load-bearing backbone in the partially molten alloy, and that the bicontinuous structure is preserved during quenching to room temperature. Samples with a contiguous porosity can be obtained by leaching the solidified melt. As extended melting intervals are ubiquitous in binary alloys, our observations provide for the innate-melt-enabled preparation of monolithic interpenetrating-phase composites or porous metals in an extended set of alloy systems.

Bicontinuous metal composites with two interpenetrating phases are of interest because of their attractive mechanical and physical properties [1–4] and since they may serve as precursors for porous metals [5–7]. This kind of composite can be obtained by spinodal decomposition [8], co-sputtering [9], selective etching and electrochemical refilling [10] or liquid metal dealloying [2,11,12]. Recently, reverse peritectic melting [13] has been found to afford through-bulk dealloying – as the intermetallic TiAg undergoes the reverse peritectic reaction, the innate melt corrodes the solid, forming a bicontinuous structure [14].

Obtaining a bicontinuous structure through reverse peritectic melting is attractive, since it requires merely a simple heat treatment and since the process – acting throughout the bulk – offers scalability to large samples. However, the approach has so far only been demonstrated for TiAg, suggesting that alloy systems with suitable peritectics may be rare. This raises the intriguing question of whether a bicontinuous structure can be obtained, alternatively, through partial melting between solidus and liquidus of solid solutions with an extended melting interval, which are ubiquitous in binary alloy systems. That might greatly enhance the applicability of innate-melt dealloying.

Solid-melt dual-phase states have been intensely studied in the field of semisolid casting [15–17]. Castability there requires not too high viscosity and, in the consequence, a disconnected solid phase. By contrast, achieving bicontinuous structures that can bear load calls for a percolating solid backbone. That condition must prevail in the partially molten state, where the microstructure is formed. It is not immediately obvious that the condition can be met, since grain boundaries are frequently observed to undergo pre-melting [18–20]. In other words, the melt tends to wet the grain boundaries, reducing the contiguity of the solid phase. A bicontinuous partly molten microstructure presupposes an alloy system with "incomplete" grain boundary wetting, that is, a system in which certain boundaries or boundary types remain at least partly dry during solid-melt coexistence.

Dry boundaries are distinguished by a nonzero contact angle at the crystal-crystal-melt triple line. Alloy systems that exhibit this phenomenon have been identified, and transition temperatures between complete and incomplete grain boundary wetting are known for various alloy systems, including Al-Mg [21], Cu-Ag [22], Al-Ga [23], Mo-Ni [24], Cu-Bi [25] and Cu-In [26–28].

Here, we explore whether bicontinuous metal alloys can be produced through partial melting. Among the above-mentioned alloy systems with incomplete grain boundary wetting, we choose Cu-In, since that system features a particularly wide interval between the start and finish temperatures of grain boundary wetting [27,28].

Our study focused on $Cu_{93}In_7$ (at.%). To prepare that alloy, Cu (>99.995%) pieces and In (>99.999%) granules were repeatedly melted together in an arc melter under Ar. The ingot was sealed in an evacuated quartz tube and homogenized at 630 °C for 7 days. For quenching,

* Corresponding author at: Institute of Materials Physics and Technology, Hamburg University of Technology, Hamburg, Germany.
E-mail address: weissmueller@tuhh.de (J. Weissmüller).

https://doi.org/10.1016/j.scriptamat.2024.116192
Received 19 April 2024; Received in revised form 20 May 2024; Accepted 21 May 2024
Available online 23 May 2024

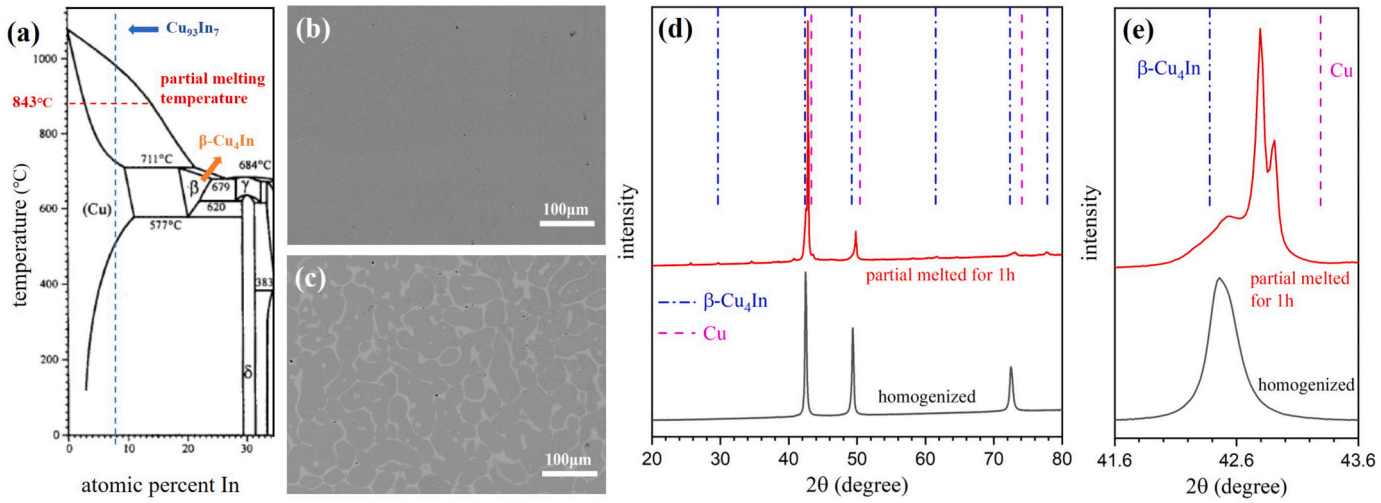

Fig. 1. Overview of the phase structure. (a), Cu-In phase diagram (after [29]). (b), backscattered electron (BSE) micrograph of $Cu_{93}In_7$ after homogenization; uniform contrast suggests single-phase alloy. (c), BSE image after partial melting for 4 min at 843 °C; two phases are clearly distinguished. (d) X-ray powder diffractogramms of scattering intensity (linear) versus scattering angle 2θ for $Cu_{93}In_7$ as homogenized (black line) and after partial melting (red line; displaced for clearer view). (e), enlarged view of diffraction near the (111) peaks. After partial melting, traces of $\beta - Cu_4In$ may be distinguished besides predominant Cu solid solution. The splitting of the (111) reflection after partial melting is from the $K_{\alpha_{1/2}}$ wavelength doublet. Reference lines from [30]. (For interpretation of the colors in the figure(s), the reader is referred to the web version of this article.)

the tube was dropped into room-temperature water and immediately broken with a hammer. Partial melting used a 5 mm diameter ceramic crucible in a furnace at air. Samples were exposed to 843 °C for various periods of time and quenched in water, with a transfer time < 2 seconds. Some samples in that condition where processed further by electrochemical dealloying in 0.5 M H_2SO_4 solution at -0.26 V against a Ag/AgCl reference electrode.

The inspection of the microstructure focused on the sample centers. All micrographs in this work are from cross-sectional surfaces, obtained by sectioning the sample after its final metallurgical or corrosion treatment. The sample segments were cold-embedded in epoxy, then ground with abrasive paper to 4000 grit and polished with colloidal silica suspension. Scanning electron microscopy (SEM) used a Zeiss Supra VP55. Samples for electron backscatter diffraction (EBSD) in the scanning electron microscope underwent the same grinding/polishing process as the SEM samples, followed by Ar ion milling for stress relief at the surface. The EBSD results were analyzed by the Channel 5 (HKL Technology, Co.) software. Coincidence Site Lattice (CSL) boundaries were distinguished automatically using the Brandon criterion [31].

Phase identification used X-ray powder diffraction in focusing Bragg-Brentano geometry, with Ni-filtered Cu Kα radiation. Samples for the diffraction experiment were ground with sand paper (1000 grit) and the so-prepared cross-sections examined.

We studied the alloy $Cu_{93}In_7$. The alloy phase diagram in Fig. 1(a) illustrates a single-phase state in a temperature interval centered around ~700 °C and an extended interval of solid-liquid coexistence at higher temperature.

Fig. 1(b) characterizes the microstructure after homogenization. The uniform gray shade suggests a single phase. Black spots represent casting pores formed upon solidification. The homogenized alloy's x-ray powder diffractogramm in Fig. 1(d) confirms the single-phase, face-centered cubic (fcc) structure, with no indication of intermetallic second phases. The Bragg reflection positions indicate a lattice parameter slightly in excess of that of Cu, consistent with the large atomic radius of the dissolved In.

The backscattered electron (BSE) image in Fig. 1(c) shows the microstructure after partial melting at 843 °C and quenching. The solid solution grains and the intergranular phase formed by the solidified alloy melt are clearly distinguished. The diffractogramm in red in Fig. 1(d) represents the sample in that state; apart from the dominant fcc reflections, the diffractogramm shows the signature of β-Cu_4In. Precipitation of that phase during quenching is consistent with the phase diagram. We conclude that at least part of the intergranular phase is β-Cu_4In.

In Fig. 1(d) and in the enlarged view around the fcc (111) Bragg reflection, Fig. 1(e), a shift of the fcc reflections to higher diffraction angles after partial melting testifies to the reduced In content (reduced lattice parameter) in the solid during solid-liquid coexistence.

In the 2D cross-sectional image of Fig. 1(c), each of the two phases – Cu rich solid solution and solidified melt – appears contiguous. Whether or not each phase is indeed contiguous in 3D may be determined based on a dealloying experiment, in which one of the phases is attacked by corrosion and converted into a porous structure. Electrochemical dealloying in 0.5 M H_2SO_4 proved efficient in dealloying selectively the solidified melt. Fig. 2 shows the microstructure in near-surface and central regions of the sample. The Cu-rich phase remains unetched, while the solidified melt has been corroded, forming a Cu-rich nanoscale network structure that resembles the typical dealloyed structure found in other alloy systems [32–34]. Obviously, In is selectively removed by our protocol.

As we find the entire intergranular phase to be corroded, we conclude that this phase was contiguous. Furthermore, the macroscopic sample remains coherent and load-bearing, evidence that the granular phase is also contiguous. In other words, the dealloying experiment confirms the suggestion of the SEM image, the partially molten microstructure is bicontinuous.

For microstructure observation in the central area of a bulk porous metal sample, the typical method is to cleave the sample with a scalpel [35]. It is noteworthy that in this study cleaving the sample after corrosion retains its structural integrity, in spite of an appreciable cutting force. This emphasizes the excellent connectivity of the granular, Cu solid solution phase.

For verifying the uniformity of the dealloyed structure throughout the sample cross-section, a sample was vacuum-embedded with epoxy and then ground and polished to reveal the central area. Indeed, the SEM observation in that state, Fig. 2(c,d) confirms the uniformity. This testifies to accessibility of the entire intergranular phase to corrosion and, hence, to its contiguity throughout the sample.

Inside the Cu solid solution grains after partial melting, BSE micrographs – such as Fig. 2(d) – exhibit small regions of bright contrast (see arrows). That contrast implies enhanced In content, suggesting regions of solidified melt. Such regions could form either by nucleation of the melt inside a grain – with, for instance, a lattice dislocation or a void as

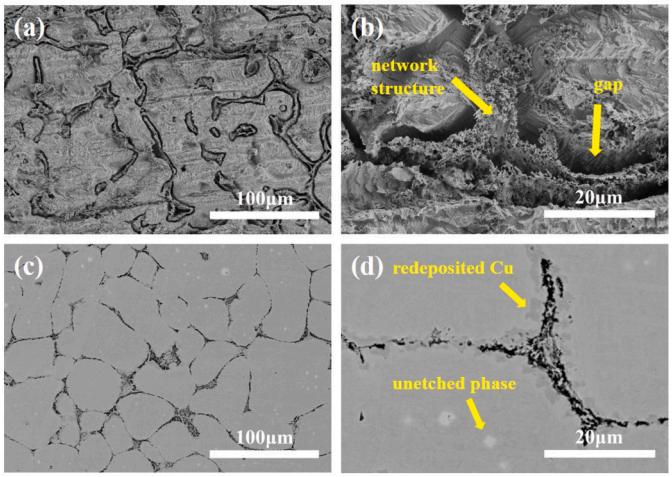

Fig. 2. Scanning electron micrographs of $Cu_{93}In_7$ after partial melting for 4 min and subsequent dealloying. (a,b): secondary electron image near the macroscopic sample surface. Intergranular phase has been converted into a nanoscale porous network structure. (c,d): back-scattered electron micrographs near the sample centre. Network structure can also be found here. Regions of redeposited Cu phase and of resolidified entrapped melt are designated by arrows.

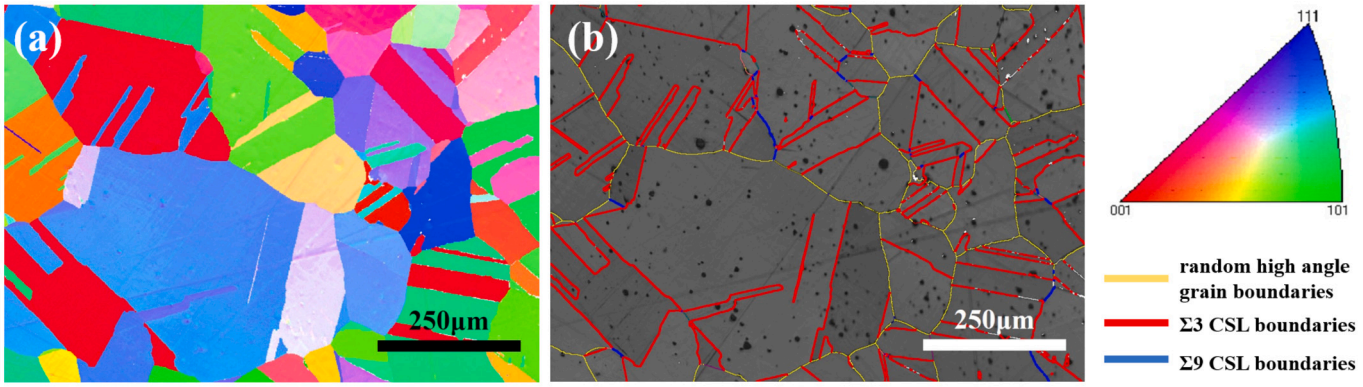

Fig. 3. Electron backscatter diffraction characterization of $Cu_{93}In_7$ after homogenization. (a) Inverse pole figure image; color indicates orientation of surface normal in stereographic standard triangle, see legend at right. (b) Boundary character map showing random high-angle grain boundaries, Σ3 coincidence site lattice boundaries and Σ9 boundaries.

the nucleation site – or by entrapment of melt during coarsening. Entrapment events in bicontinuous microstructures are well known from coarsening of dealloyed porous metals, where they convert part of the contiguous pore space into isolated voids [36,37].

Figs. 2 (a) and (b) show gaps between the Cu-rich solid solution grains and the dealloyed porous regions. Quite similar features are routinely observed at the interface between dealloyed nanoporous gold and massive gold substrates [38]. They can be explained by transport of the constituent of the pore network (Au, in those studies) towards regions of reduced mean curvature at the substrate. The mean curvature of the pore surfaces gives rise to a Gibbs-Thompson excess in chemical potential. Curvature gradients near the substrate prompt a divergence in the diffusive flux; this results in the depletion of the near-interface network region in Au and eventually in the formation of a gap [38]. This mechanism would seem to be transferable to Cu diffusion in the present situation, with the granular phase assuming the role of the substrate.

In the BSE image of Fig. 2(d), laterally confined regions of a darker contrast are apparent at the surface of the granular phase after dealloying. As the darker contrast is associated with higher content in Cu, those regions might represent pure Cu that was redeposited during dealloying. The redeposition, which was also observed in earlier dealloying studies [39,40], may again be understood as the consequence of excess chemical potential of Cu in the nanoporous structure. According to this hypothesis, the Cu redeposits preferentially in concave regions of the solid-solution grain surface. The high magnification SEM image in Fig S1 of the Supporting Information illustrates wavy surface segments, including concave regions, after partial melting and prior to dealloying.

We have performed EBSD for mapping grain boundary characters in the as-homogenized and in the quenched-after-partial-melting states. Fig. 3(a) shows the EBSD image of the grain structure in the as-homogenized alloy, with randomly oriented and curved or serrated lines suggesting high angle grain boundaries and straight, parallel lines suggesting twins. Fig. 3(b) displays the grain boundary characters. High-angle boundaries (misorientation > 15 degree) are the predominant boundary type. They include (in red) a large proportion of Σ3 Coincidence Site Lattice (CSL) boundaries – that is, twin boundaries – and (in blue) occasional Σ9 boundaries which are geometrically related to Σ3 boundaries [41]. The remaining grain boundaries (in yellow) are categorized as random high-angle grain boundaries.

Next, let us inspect EBSD data for the alloy after partial melting (here for 4 min) and re-solidification, Fig. 4. The grain boundary character map, Fig. 4(b), reveals random high angle grain boundaries as well as Σ3, Σ9, Σ11 and Σ27. As the image gives no evidence for molten regions at those grain boundaries, it confirms that boundaries from that set of characters can remain dry at the temperature of our anneal. Specifically, non-wetted high-angle grain boundaries were found to prevail even after extended anneals in the partially molten state, see the EBSD image after 1 h of annealing, Fig S2 in the Supporting Information.

Straumal et al. [26,28] have shown that the wetting transition temperature, above which the contact angle vanishes (complete wetting),

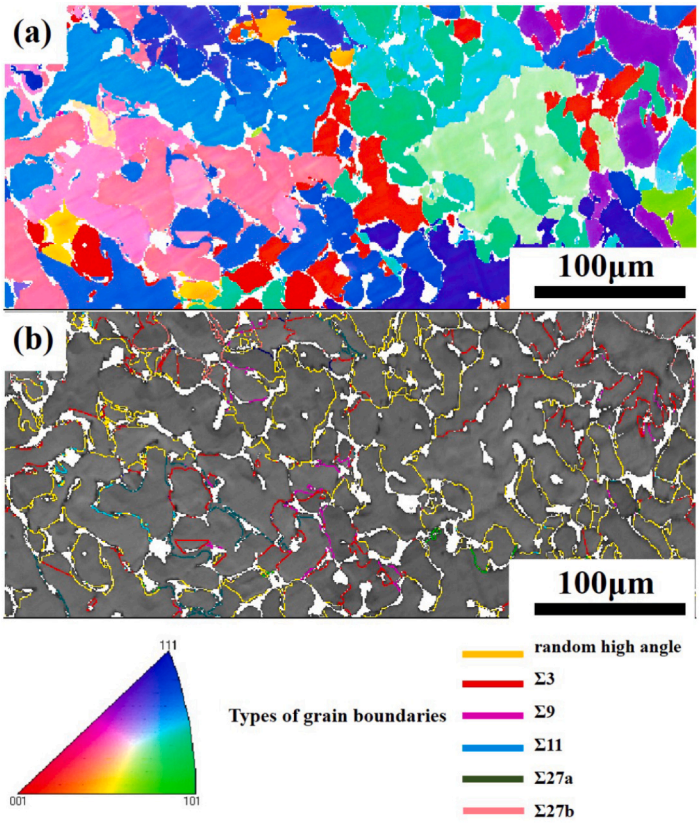

Fig. 4. Electron backscatter diffraction maps of $Cu_{93}In_7$ alloy after partial melting for 4 min. (a) Inverse pole figure image; color indicates orientation of surface normal in stereographic standard triangle, see legend at bottom. (b) Boundary information, showing retention of random high-angle grain boundaries as well as various types of CSL boundaries after partial melting.

is closely related to the specific grain boundary energy, γ. As compared to random high-angle grain boundaries, CSL boundaries, especially the low-γ boundary Σ3, require a higher temperature to be completely wetted [42]. The temperature range between the start and finish of complete wetting in the set of all boundaries in Cu-In is from 715 °C to 986 °C [27]. Those findings suggest that some boundaries will remain incompletely wetted in the partial melting state at 843 °C. It is not readily obvious what fraction of incompletely wetted grain boundaries is required for retaining a contiguous solid phase. Yet, the mechanical robustness of the dealloyed sample indicates that enough incompletely wetted grain boundaries were left after partial melting.

Besides the grain boundary character, the grain microstructure in Fig. 4 is also remarkable. Clusters of granular features exhibit a common grain orientation, penetrated by multiple solidified melt channels. The clusters (grains) have similar size as the grains in the master alloy (several hundred micrometers), Fig. 3, whereas the individual granular regions are substantially smaller (around 30 μm after partial melting for 4 min). This provides an incentive for inspecting the evolution of the microstructure as the time at two-phase coexistence is varied.

Fig. 5 displays the microstructure evolution after partial melting for different times, from 1 min to 1 h before and after dealloying. As the most obvious observation, the microstructural length-scale is seen to increase significantly with time. That is readily understandable as curvature-driven coarsening, mediated by fast diffusion through the melt.

More intriguing is the observation that, for the shortest time (1 min) at solid-liquid coexistence, the characteristic feature size is actually smaller than the grain size of the original homogenized alloy (see Fig. 3). That observation can be traced to the mechanism by which the microstructure equilibrates in the dual-phase state. The fastest transport mechanism is not solid-state diffusion of the excess indium from the solid solution in the grain interior to the initial, molten film at the nearest grain boundary. Instead, wetted grain boundaries can migrate and sweep the grain interior, leaving equilibrated solid solution behind. This discontinuous reaction by interface migration [43] is an established analogon to diffusion-induced grain boundary migration [44].

Liquid film migration and the discontinuous precipitation of the equilibrated phase have seen dedicated studies for Cu-In [45,46]. The process can refine the microstructure, since the free energy gain associated with the reaction can overcompensate the energy expenditure from increasing the area of the liquid film's interfaces. As the solidification behind the migrating interface redeposits matter on the crystal lattice of existing grains, the discontinuous precipitation by liquid film migration is consistent with our observation of clusters containing several crystallographically aligned crystals that are separated by (solidified) liquid films. The absence of Kirkendall voids in the granular phase of Fig. 5(a) is consistent with a negligible contribution of solid-state diffusion.

All samples of Fig. 5 exhibit voids in the intergranular phase. We tentatively attribute those voids to volume shrinkage during solidification.

Fig. 5(e-h) present the microstructure of samples with different partial melting time, after dealloying. The intergranular phase appears completely dealloyed in each sample. This indicates that the liquid phase is already interconnected after partial melting for only 1 min, and that it remained interconnected during a prolonged hold at the partial melting temperature.

The alloy $Cu_{93}In_7$ is studied in this research to show that a bicontinuous microstructure can be obtained by partial melting in the solid-liquid coexistence region. Unwetted boundaries in Cu solution phase provide the connectivity of the solid phase at high temperature. The obtained structure is the result of the liquid film migration as well as the subsequent coarsening. The bicontinuous microstructure achieved at elevated temperatures can be preserved through rapid quenching in water. For the $Cu_{93}In_7$ alloy, both the Cu solid solution and the β-Cu_4In

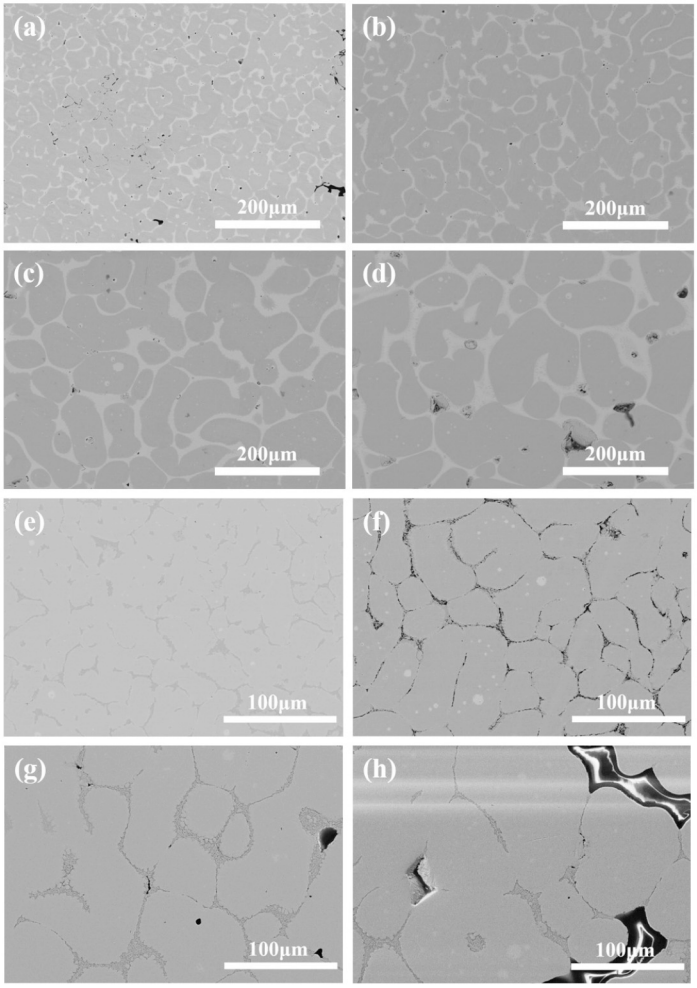

Fig. 5. Scanning electron micrographs (BSE) exploring the microstructure after partial melting at 843 °C for (a) 1 min; (b) 4 min; (c) 15 min; (d) 1 h before dealloying. An obvious increase in the size of both phases with prolonged melting time can be observed. Microstructure of dealloyed $Cu_{93}In_7$ alloy (BSE images) with different partial melting time: (e) 1 min; (f) 4 min; (g) 15 min; (h) 1 h. Note that the nanoscale net work structure was found in the central area of all samples. This shows that solidified melt phase remained continuous after prolonged partial melting time.

phase remain interconnected after the partial melting process from 1 min to 1 h. This method introduces a novel and easy approach to fabricate bulk bicontinuous metal composites or porous metals, with the potential of becoming a universal synthesizing method for many different alloy systems.

CRediT authorship contribution statement

Zhongyang Li: Writing – original draft, Methodology, Investigation, Conceptualization. **Lukas Lührs:** Writing – review & editing, Conceptualization. **Jörg Weissmüller:** Writing – review & editing, Conceptualization.

Declaration of competing interest

The corresponding author confirms on behalf of all authors that there have been no involvements that might raise the question of bias in the work reported or in the conclusions, implications, or opinions stated.

Acknowledgement

This work was supported by the Deutsche Forschungsgemeinschaft (DFG) within the Collaborative Research Centre CRC 986 “Tailor-Made Multi-Scale Materials Systems” (Project No. 192346071) and by the China Scholarship Council.

Appendix. Supplementary material

Supplementary material related to this article can be found online at https://doi.org/10.1016/j.scriptamat.2024.116192.

References

[1] I. McCue, B. Gaskey, B. Crawford, J. Erlebacher, Local heterogeneity in the mechanical properties of bicontinuous composites made by liquid metal dealloying, Appl. Phys. Lett. 109 (2016).
[2] I. McCue, S. Ryan, K. Hemker, X.D. Xu, N. Li, M.W. Chen, J. Erlebacher, Size effects in the mechanical properties of bulk bicontinuous Ta/Cu nanocomposites made by liquid metal dealloying, Adv. Eng. Mater. 18 (2016) 46–50.
[3] C. Soyarslan, M. Pradas, S. Bargmann, Effective elastic properties of 3D stochastic bicontinuous composites, Mech. Mater. 137 (2019) 103098.
[4] Y.C. Cui, B. Derby, N. Li, A. Misra, Design of bicontinuous metallic nanocomposites for high-strength and plasticity, Mater. Des. 166 (2019) 107602.
[5] X. Guo, C. Zhang, Q. Tian, D. Yu, Liquid metals dealloying as a general approach for the selective extraction of metals and the fabrication of nanoporous metals: a review, Materials Today Communications 26 (2021) 102007.
[6] L. Lai, B. Gaskey, A. Chuang, J. Erlebacher, A. Karma, Topological control of liquid-metal-dealloyed structures, Nat. Commun. 13 (2022) 2918.
[7] T. Wada, K. Yubuta, H. Kato, Evolution of a bicontinuous nanostructure via a solid-state interfacial dealloying reaction, Scr. Mater. 118 (2016) 33–36.

[8] H. Jinnai, Y. Nishikawa, T. Koga, T. Hashimoto, Direct observation of three-dimensional bicontinuous structure developed via spinodal decomposition, Macromolecules 28 (1995) 4782–4784.
[9] N. Beets, Y.C. Cui, D. Farkas, A. Misra, Mechanical response of a bicontinuous copper–molybdenum nano-composite: experiments and simulations, Acta Mater. 178 (2019) 79–89.
[10] H. Guan, H. Xie, Z.P. Luo, W.K. Bao, Z.S. You, Z. Jin, H.J. Jin, Ultrastrong spinodoid alloys enabled by electrochemical dealloying and refilling, Proc. Natl. Acad. Sci. 120 (2023) e2214773120.
[11] Y.B. Jeong, T. Wada, S.H. Joo, J.M. Park, J. Moon, H.S. Kim, I.V. Okulov, S.H. Park, J.H. Lee, K.B. Kim, et al., Beyond strength-ductility trade-off: 3D interconnected heterostructured composites by liquid metal dealloying, Composites, Part B, Eng. 225 (2021) 109266.
[12] I.V. Okulov, J. Wilmers, S.H. Joo, S. Bargmann, H.S. Kim, H. Kato, Anomalous compliance of interpenetrating-phase composite of Ti and Mg synthesized by liquid metal dealloying, Scr. Mater. 194 (2021) 113660.
[13] M. Hillert, L. Höglund, Melting of a peritectic phase, Scr. Mater. 50 (2004) 1055–1059.
[14] W.K. Hu, J.C. Shao, S.G. Wang, H.J. Jin, Evolution of a bicontinuous structure in peritectic melting: the simplest form of dealloying, Phys. Rev. Mater. 3 (2019) 113601.
[15] J.K. Ren, M.Y. Sun, Y. Chen, B. Xu, W.F. Liu, H.Y. Jiang, Y.F. Cao, D.Z. Li, The non-dendritic microstructure arising from grain boundary formation and wetting: a phase-field simulation and experimental investigation of semi-solid deformation, Mater. Des. 223 (2022) 111111.
[16] K.N. Campo, C.C. de Freitas, S.C. Moon, R. Dippenaar, R. Caram, In-situ microstructural observation of Ti-Cu alloys for semi-solid processing, Mater. Charact. 145 (2018) 10–19.
[17] J.Y. Li, S. Sugiyama, J. Yanagimoto, Y.L. Chen, G.W. Fan, Effect of inverse peritectic reaction on microstructural spheroidization in semi-solid state, J. Mater. Process. Technol. 208 (2008) 165–170.
[18] E. Glickman, M. Nathan, On the kinetic mechanism of grain boundary wetting in metals, J. Appl. Phys. 85 (1999) 3185–3191.
[19] M. Takashima, P. Wynblatt, B. Adams, Correlation of grain boundary character with wetting behavior, Interface Sci. 8 (2000) 351–361.
[20] J. Sun, Y. Zhang, A. Lyckegaard, F. Bachmann, E. Lauridsen, D.J. Jensen, Grain boundary wetting correlated to the grain boundary properties: a laboratory-based multimodal X-ray tomography investigation, Scr. Mater. 163 (2019) 77–81.
[21] B. Straumal, O. Kogtenkova, M.Y. Murashkin, M. Bulatov, T. Czeppe, P. Zięba, Grain boundary wetting transition in Al–Mg alloys, Mater. Lett. 186 (2017) 82–85.
[22] I. Mazilkin, K. Tsoy, A. Straumal, A. Rodin, B. Baretzky, Grain boundary wetting of different types of grain boundaries in the Cu–Ag system, Mater. Lett. 272 (2020) 127730.
[23] W. Ludwig, E. Pereiro-López, D. Bellet, In situ investigation of liquid Ga penetration in Al bicrystal grain boundaries: grain boundary wetting or liquid metal embrittlement?, Acta Mater. 53 (2005) 151–162.
[24] X.M. Shi, J. Luo, Grain boundary wetting and prewetting in Ni-doped Mo, Appl. Phys. Lett. 94 (2009).
[25] K. Wolski, V. Laporte, Grain boundary diffusion and wetting in the analysis of intergranular penetration, Mater. Sci. Eng. A 495 (2008) 138–146.
[26] B. Straumal, T. Muschik, W. Gust, B. Predel, The wetting transition in high and low energy grain boundaries in the Cu (In) system, Acta Metall. Mater. 40 (1992) 939–945.
[27] A. Straumal, B. Bokstein, A. Petelin, B. Straumal, B. Baretzky, A. Rodin, A. Nekrasov, Apparently complete grain boundary wetting in Cu–In alloys, J. Mater. Sci. 47 (2012) 8336–8343.
[28] A.B. Straumal, V.A. Yardley, B.B. Straumal, A.O. Rodin, Influence of the grain boundary character on the temperature of transition to complete wetting in the Cu–In system, J. Mater. Sci. 50 (2015) 4762–4771.
[29] A. Bolcavage, S. Chen, C. Kao, Y. Chang, A. Romig, Phase equilibria of the Cu-In system I: experimental investigation, J. Phase Equilib. 14 (1993) 14–21.
[30] Z. Bahari, E. Dichi, B. Legendre, J. Dugué, The equilibrium phase diagram of the copper–indium system: a new investigation, Thermochim. Acta 401 (2003) 131–138.
[31] D. Brandon, The structure of high-angle grain boundaries, Acta Metall. 14 (1966) 1479–1484.
[32] B. Zandersons, L. Lührs, Y. Li, J. Weissmüller, On factors defining the mechanical behavior of nanoporous gold, Acta Mater. 215 (2021) 116979.
[33] S. Shi, J. Markmann, J. Weissmüller, Synthesis of uniform bulk nanoporous palladium with tunable structure, Electrochim. Acta 285 (2018) 60–69.
[34] L.Y. Chen, J.S. Yu, T. Fujita, M.W. Chen, Nanoporous copper with tunable nanoporosity for SERS applications, Adv. Funct. Mater. 19 (2009) 1221–1226.
[35] G. Wittstock, M. Bäumer, W. Dononelli, T. Klüner, L. Lührs, C. Mahr, L.V. Moskaleva, M. Oezaslan, T. Risse, A. Rosenauer, et al., Nanoporous gold: from structure evolution to functional properties in catalysis and electrochemistry, Chem. Rev. 123 (2023) 6716–6792.
[36] H. Rösner, S. Parida, D. Kramer, C.A. Volkert, J. Weissmüller, Reconstructing a nanoporous metal in three dimensions: an electron tomography study of dealloyed gold leaf, Adv. Eng. Mater. 9 (2007) 535–541.
[37] J. Erlebacher, Mechanism of coarsening and bubble formation in high-genus nanoporous metals, Phys. Rev. Lett. 106 (2011) 225504.
[38] G. Henkelmann, D. Waldow, M. Liu, L. Lührs, Y. Li, J. Weissmüller, Self-detachment and subsurface densification of dealloyed nanoporous thin films, Nano Lett. 22 (2022) 6787–6793.
[39] R. Li, N. Wu, J.J. Liu, Y. Jin, X.B. Chen, T. Zhang, Formation and evolution of nanoporous bimetallic Ag-Cu alloy by electrochemically dealloying Mg-(Ag-Cu)-Y metallic glass, Corros. Sci. 119 (2017) 23–32.
[40] L. Yang, Y.Q. Shi, L.J. Shen, E.L. Zhang, G.W. Qin, X.P. Lu, X.R. Zhou, Effect of Ag on cathodic activation and corrosion behaviour of Mg-Mn-Ag alloys, Corros. Sci. 185 (2021) 109408.
[41] V. Randle, Y. Hu, M. Coleman, Grain boundary reorientation in copper, J. Mater. Sci. 43 (2008) 3782–3791.
[42] J.M. Howe, Physical Metallurgy, Elsevier, 2014, pp. 1317–1451.
[43] I. Manna, S.K. Pabi, W. Gust, Discontinuous reactions in solids, Int. Mater. Rev. 46 (2001) 53–91.
[44] R.W. Balluffi, J.W. Cahn, Mechanism for diffusion induced grain boundary migration, Acta Metall. 29 (1981) 493–500.
[45] T. Muschik, W. Kaysser, T. Hehenkamp, Melting of Cu-In solid solutions at small superheating by droplet formation and liquid film migration, Acta Metall. 37 (1989) 603–613.
[46] S.P. Gupta, S.K. Goutam, P. Suresh Babu, Discontinuous precipitation of a liquid in Cu-base alloys–nucleation and growth mechanisms, Int. J. Mater. Res. 94 (2022) 442–448.